Robust Digital Molecular Design of Binarized Neural Networks

Johannes Linder
University of Washington, Paul G. Allen School of Computer Science and Engineering, Seattle, WA, USA

Yuan-Jyue Chen
Microsoft Research, Redmond, WA, USA

David Wong
University of Washington, Department of Bioengineering, Seattle, WA, USA

Georg Seelig
University of Washington, Paul G. Allen School of Computer Science and Engineering, Seattle, WA, USA
University of Washington, Department of Electrical and Computer Engineering, Seattle, WA, USA

Luis Ceze
University of Washington, Paul G. Allen School of Computer Science and Engineering, Seattle, WA, USA

Karin Strauss
Microsoft Research, Redmond, WA, USA
University of Washington, Paul G. Allen School of Computer Science and Engineering, Seattle, WA, USA

Abstract

Molecular programming – a paradigm wherein molecules are engineered to perform computation – shows great potential for applications in nanotechnology, disease diagnostics and smart therapeutics. A key challenge is to identify systematic approaches for compiling abstract models of computation to molecules. Due to their wide applicability, one of the most useful abstractions to realize is neural networks. In prior work, real-valued weights were achieved by individually controlling the concentrations of the corresponding "weight" molecules. However, large-scale preparation of reactants with precise concentrations quickly becomes intractable. Here, we propose to bypass this fundamental problem using Binarized Neural Networks (BNNs), a model that is highly scalable in a molecular setting due to the small number of distinct weight values. We devise a noise-tolerant digital molecular circuit that compactly implements a majority voting operation on binary-valued inputs to compute the neuron output. The network is also rate-independent, meaning the speed at which individual reactions occur does not affect the computation, further increasing robustness to noise. We first demonstrate our design on the MNIST classification task by simulating the system as idealized chemical reactions. Next, we map the reactions to DNA strand displacement cascades, providing simulation results that demonstrate the practical feasibility of our approach. We perform extensive noise tolerance simulations, showing that digital molecular neurons are notably more robust to noise in the concentrations of chemical reactants compared to their analog counterparts. Finally, we provide initial experimental results of a single binarized neuron. Our work suggests a solid framework for building even more complex neural network computation.

2012 ACM Subject Classification Theory of computation → Models of computation; Applied computing

Keywords and phrases Molecular Computing, Neural Network, Binarized Neural Network, Digital Logic, DNA, Strand Displacement

Digital Object Identifier 10.4230/LIPIcs.DNA.27.1

1 Introduction

Computing in molecules is a prerequisite for a wide range of potentially revolutionizing nanotechnologies, such as molecular nanorobots and smart therapeutics. For example, molecular "programs" delivered to cells could collect sensory input from gene expression to determine the prevalence of disease and conditionally release a drug. Molecular disease classifiers have already been demonstrated outside of cells [1, 18]. Moreover, as researchers look toward synthetic DNA for storing data [9, 20, 4], it becomes increasingly important to develop operations that can be executed on data in molecular form.

Bringing such applications closer to reality requires abstractions and programming languages that can capture the desired molecular behaviors. A methodical way to reason about chemical computing is through the formalism of chemical reaction networks (CRNs). A CRN is a collection of coupled chemical reactions, each consuming a set of reactants to create a set of products. CRNs are Turing universal [27, 12] and any CRN can in principle be implemented using synthetic DNA molecules, specifically DNA strand displacement [28, 7].

Molecular computing has traditionally been approached from two different design philosophies; in *analog* computing, the numerical value of each variable is encoded in the concentration of its corresponding molecular species [24, 5, 33]. Conversely, in *digital* molecular computing, concentrations of species representing logical values are restricted to "high" or "low" ranges similar to voltages in digital electronics [13, 19]. Feed-forward neural networks have previously been demonstrated as analog molecular circuits [34, 23, 6, 8, 32]. While compact, analog molecular circuits are inherently sensitive to concentration noise, as such perturbation directly impacts the correctness of the system.

Here, we develop a digital molecular implementation of binarized neural networks, a class of models where the inputs, weights and activations are constrained to take the values $\{+1, -1\}$ [14]. We devise an efficient molecular circuit for computing binary n-input majority using $\mathcal{O}(n^2)$ gates and $\mathcal{O}(\log n)$ (optimal) depth. Each neuron uses this circuit for their weighted sum and threshold operation. This design offers a uniquely scalable molecular implementation: while an analog monotonic network requires exponentially large concentrations of molecular substrates as a function of layer depth to avoid saturation of outputs (we develop this argument in Section 3), our design uses a constant concentration across all network layers. We demonstrate our design on the MNIST task, both as idealized CRNs and as DNA strand displacement cascades. Finally, we compare the digital neuron to an analog, rate-independent HardTanh-activated neuron and present improved robustness to concentration noise and leak. We also present initial experimental results of a simple 2-input binarized neuron.

2 Background

2.1 Binarized Neural Networks

In this paper we focus on deterministic binarized neural networks (BNNs) as described by [14]. If we first consider a single neuron, its inputs x_i, weights w_i, bias term b and activation y are binary-valued and constrained to $\{+1, -1\}$. We compute neuron activation y as:

$$y = \begin{cases} +1 & \text{if } b + \sum_{i=1}^{N} w_i \cdot x_i > 0 \\ -1 & \text{else} \end{cases} \tag{1}$$

Binarized neurons are assembled into fully connected neural networks by treating output y of a neuron i in layer k as the input x_i to neuron j of layer $k+1$, connected through weight $w_{ij}^{(k)} \in \{+1, -1\}$. BNNs can be efficiently trained by gradient descent following the scheme of the original authors, where a straight-through estimator was used to propagate gradients through binarized non-linearities. While BNNs usually are less accurate than their full-precision counterparts, they offer substantial improvements in execution time and storage space [26]. Since BNN computation can be executed with bitwise operations, they are also amenable to efficient implementation on FPGAs and ASICs. Recent BNN architectures show relatively good performance on more complex tasks such as ImageNet classification [10].

2.2 Chemical Reaction Networks

Chemical Reaction Networks (CRNs) are a mathematical formalism traditionally used by chemists to describe how the concentration or counts of chemical species evolve over time. Two example reactions are shown below:

$$A + B \rightarrow C$$
$$C \rightarrow D + E$$

Reaction 1 dictates that one molecule each of A and B react to produce C, until A or B are fully consumed. Reaction 2 consumes one molecule of C to produce one molecule each of D and E. Commonly, a rate constant that captures how fast an instance of a reaction occurs is also associated with each reaction. In this paper, we consider reactions with at most two reactants or two products. When modeling the time evolution of CRNs, we often reason about concentrations. We denote the concentration of A at time t as $a(t)$. Assuming mass action kinetics, $a(t)$ can be modeled as an ODE [11].

Analog and Digital CRNs

Molecular programming with CRNs can be approached from different computational models. Two of the most widely used models are *analog* CRNs and *digital* CRNs. In analog CRNs, any non-negative real-valued variable $x \in \mathbb{R}^+$ is represented by a corresponding molecular species X. The value of x is encoded in the concentration $x(t)$ [24]. For example, $x = 3.2$ is represented as $x(t) = 3.2\text{nM}$. This convention makes summation trivial to implement; to compute $s = \sum_{i=1}^{N} x_i$, we add N reactions translating species X_i to the same species S:

$$X_i \rightarrow S \quad , 1 \leq i \leq N$$

As time progresses, each input X_i accumulates in species S such that $t \rightarrow \infty$ $s(t) = \sum_{i=1}^{N} x_i(0)$.

In a digital computing paradigm, we restrict variables to be discrete, such that they can only take on a finite number of states. Each discrete variable and state is encoded by its own molecular species (e.g. Boolean variable x is encoded by two species, $X^{(\text{on})}$ and $X^{(\text{off})}$). Chemical concentrations represent only high or low signals indicating which state is active. For example, Boolean variable x is modeled by the following CRN convention (Here $T^{(\text{high})}$ is a constant representing the signal filter cutoff and the third case represents incorrect states):

$$x = \begin{cases} \text{on} & \text{if } x^{(\text{on})}(t) \geq T^{(\text{high})} \text{ and } x^{(\text{off})}(t) < T^{(\text{high})} \\ \text{off} & \text{if } x^{(\text{on})}(t) < T^{(\text{high})} \text{ and } x^{(\text{off})}(t) \geq T^{(\text{high})} \\ \text{(undefined)} & \text{else} \end{cases}$$

Note that N-input summation is more complicated under this paradigm, as inputs can no longer simply be translated to the same output species to encode logical sum. Instead, proper digital circuits such as carry adders have been implemented as CRNs [16, 22].

Piecewise Linear CRNs and HardTanh

In analog CRNs, a real-valued variable $x \in \mathbb{R}$ that can take on negative values is often represented in dual-rail form by two species X^- and X^+. The value of x is encoded as the difference in their concentration, $x = \lim_{t\to\infty} x^+(t) - x^-(t)$. Using this convention, the function $h = \max(x, -k)$ can be implemented by two reactions [5] (the initial concentration of K is set to $k(0) = k$ and $x^+(0)$, $x^-(0)$ are initialized such that $x^+(0) - x^-(0) = x$):

$$\begin{aligned} X^+ &\to H^+ + K \\ X^- + K &\to H^- \end{aligned} \tag{2}$$

Similarly, function $y = \min(h, m)$ can be implemented as (here $m(0) = m$ etc.):

$$\begin{aligned} H^- &\to Y^- + M \\ H^+ + M &\to Y^+ \end{aligned} \tag{3}$$

Note that $k, m \in \mathbb{R}^+$, so dual-rail is not needed to express their values. By stacking these two sets of reactions and setting $k(0) = 1$ and $m(0) = 1$, we can implement a rate-independent, analog HardTanh function, $y = \min(\max(x, -1), 1)$. We use this construction below when comparing the digital neuron developed in this paper to a HardTanh-activated neuron based on analog CRNs, which is similar to the ReLU (Rectified Linear Unit) network by [32].

2.3 DNA Strand Displacement

Toehold-mediated DNA strand displacement (DSD) is a framework capable of synthesizing any CRN [28, 7, 30]. Molecular species are compiled into signal strands which react through synthetic DNA gates as specified by the CRN reactions. In this paper we use the *two-domain* architecture from [3], which supports all of the functionality needed to implement our digital BNN design; the gates can be prepared at large scale from double-stranded DNA by enzymatic processing and the architecture supports AND-logic, catalytic amplification and fan-out operations.

Two-domain gates work by exposing a toehold which, when hybridized by an input strand, triggers a sequence of displacements. These displacements ultimately release the output strand bound to the gate. As an example, consider the simple CRN reaction $A \to B$. The corresponding two-domain DSD system is shown in Figure 1. Species A is represented by the signal strand to the left (domains t and a – abbreviated *ta*) and B is represented by the strand with domains b and f (*bf*). A sequence of displacements mediated by toehold t eventually releases the output strand from the gate. Specifically, the sequence of displacements are:

1. Input strand *ta* binds to gate *G*, displacing strand *at* and exposing inner toehold *t*. (Reversible reaction)
2. Helper strand *tb* binds to the newly opened toehold, displacing output strand *bf* and exposing inner toehold *f*. (Reversible reaction)
3. Helper strand *fw* binds to the newly opened toehold, displacing strand *w* and closing gate *G*. (Irreversible reaction)

A promising alternative for synthesizing CRNs is Polymerase-mediated strand displacement (PSD), where polymerase enzymes trigger initially single-stranded DNA gates by extending hybridized input strands and consequently displacing any output strand [29, 25]. In this paper, we focus solely on implementing the neural network with enzyme-free toehold-mediated DSD, but we discuss implementation with PSD towards the end.

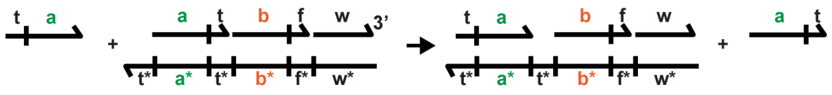

Figure 1 Input strand *ta* releases strand *at* and exposes new toehold t. Additional steps of strand displacement (not shown) ultimately release output strand *bf*. Additional helper strands *tb* and *fw* (not shown) help carry out the sequence of displacement reactions.

3 Related Work

Neural networks with real-valued weights based on analog computation have previously been built with DNA strand displacement cascades [23, 8, 6]. Non-linear activation was achieved by introducing threshold gates with much faster reaction rates than gates producing an output signal. A recent paper by [32] proposed a rate-independent analog CRN to implement a neural network with binary-valued weights and ReLU activations.

Neural networks based on monotonic analog CRNs may require exponentially large concentrations of molecular substrates at deeper network layers to avoid saturation. To see why, assume a binary-weighted, ReLU-activated network consisting of K layers and N neurons per layer. If we set all weights w_{ij}^k to $+1$ and all inputs x_i^0 to $+1$, then each activation in the first layer becomes:

$$x_j^1 = \max\Big(\sum_{i=1}^{N} w_{ij}^0 \cdot x_i^0, 0\Big) = N.$$

To physically implement this computation, we require a DSD gate or other substrate that can produce the molecular species for x_j^1 at a concentration N times larger than x_i^0. Inductively, at the final layer, each activation x_j^K can be as large as N^K, requiring gates with concentrations proportional to N^K to avoid saturation. We can similarly construct a worst-case example for the HardTanh function from the previous section; by setting half the weights w_{ij}^k to $+1$ and half the weights to -1, the concentration of output species Y^+ / Y^- of Reaction Set 3 will be $N/2$. With the same inductive argument as before, we need gate concentrations proportional to $(N/2)^K$ to avoid saturation.

Our design differs from that of [23] and [32] in that the CRN computation is carried out with digital logic. Since concentrations are used only to represent high or low signals, the computation remains correct under perturbation, similar in concept to how electronic digital circuits offer more robust behavior than analog electronic circuits. The digital design also makes the system rate-independent and allows for a uniform gate concentration across all network layers.

4 A Digital Molecular Implementation of Binarized Neurons

A binarized neuron with inputs $x_i \in \{+1, -1\}$, weights $w_i \in \{+1, -1\}$ and bias $b \in \{+1, -1\}$ is illustrated in Figure 2A. To simplify the implementation, we assume the number of inputs, N, is a power of 2. The neuron consists of a sequence of three operations:

1. Weight operations $s_i^0 = w_i \cdot x_i$, where s_i^0 denotes weighted input i before summation.
2. A sum operation $s = \sum_{i=1}^{N} s_i^0$.
3. A sign operation $y = \text{sign}(s + b)$, where b breaks ties in the case when $s = 0$.

Alternatively, steps 2 and 3 may be considered a majority voting operation between positive and negative inputs. The following sections describe how we implement the computational graph shown in Figure 2B of a digital neuron with chemical reactions. We only discuss a single neuron here to keep the notation light, but a generalization to an arbitrarily sized BNN is described in Appendix A.

4.1 Weight

Each input x_i is represented by two CRN species, X_i^+ and X_i^-, corresponding to states $x_i = +1$ and $x_i = -1$ respectively. We implement the weight operation $s_i^0 = w_i \cdot x_i$ as follows (Figure 2C): If $w_i = +1$, we add catalytic reactions translating the **positive-state** input species X_i^+ to the **positive-state** weighted species $S_i^{0,+}$, and we similarly translate X_i^- to $S_i^{0,-}$.

$$\begin{aligned} X_i^+ &\to X_i^+ + S_i^{0,+} \\ X_i^- &\to X_i^- + S_i^{0,-} \end{aligned}$$

If $w_i = -1$, we instead translate X_i^+ to $S_i^{0,-}$, and vice versa for the negative-state input species.

$$\begin{aligned} X_i^+ &\to X_i^+ + S_i^{0,-} \\ X_i^- &\to X_i^- + S_i^{0,+} \end{aligned}$$

In practice, the catalytic reactions do not replenish the input species indefinitely, but rather transform some gate substrate G into waste W (e.g. $X + G \to X + W + Y$ for input species X and output Y), but this does not matter for our theoretical analysis.

4.2 Majority Vote

If there are more weighted species $s_i^0 = w_i \cdot x_i$ in a positive state than a negative state, the circuit should output a positive state, and vice versa. We can easily enumerate every such rule as a chemical reaction of N-ary AND-clauses, given the CRN species $S_i^{0,+}$ and $S_i^{0,-}$ of each weighted input. For example, to handle the case $\mathbf{s}^0 = \mathbf{w} * \mathbf{x} = (+1, +1, +1, -1)$, we would add the reaction:

$$S_1^{0,+} + S_2^{0,+} + S_3^{0,+} + S_4^{0,-} \to Y^+$$

This CRN is problematic for two reasons: First, the number of reactions grows exponentially with N. Second, the CRN requires arbitrary-length AND-clauses, which is not feasible when implemented as DNA strand displacement gates. Instead, we here devise an efficient digital majority voting CRN that requires only a quadratic number of gates and a logarithmic (optimal) depth. We will compute the sum $s = \sum_{i=1}^{N} s_i^0$ as a balanced tree of binary additions using a recursive definition (Figure 2B):

$$s_h^k = s_{2h-1}^{k-1} + s_{2h}^{k-1}$$

Here $k = 1, \ldots, \log(N)$ and $h = 1, \ldots, N/2^k$. At level $k = \log(N)$, the full sum s is stored in $s_1^{\log(N)}$. For each binary addition performed during the recursion, we will add chemical reactions translating every possible combination of discrete values of s_{2h-1}^{k-1} and s_{2h}^{k-1} into the species of s_h^k corresponding to their sum. Suppose the summands can take on m discrete

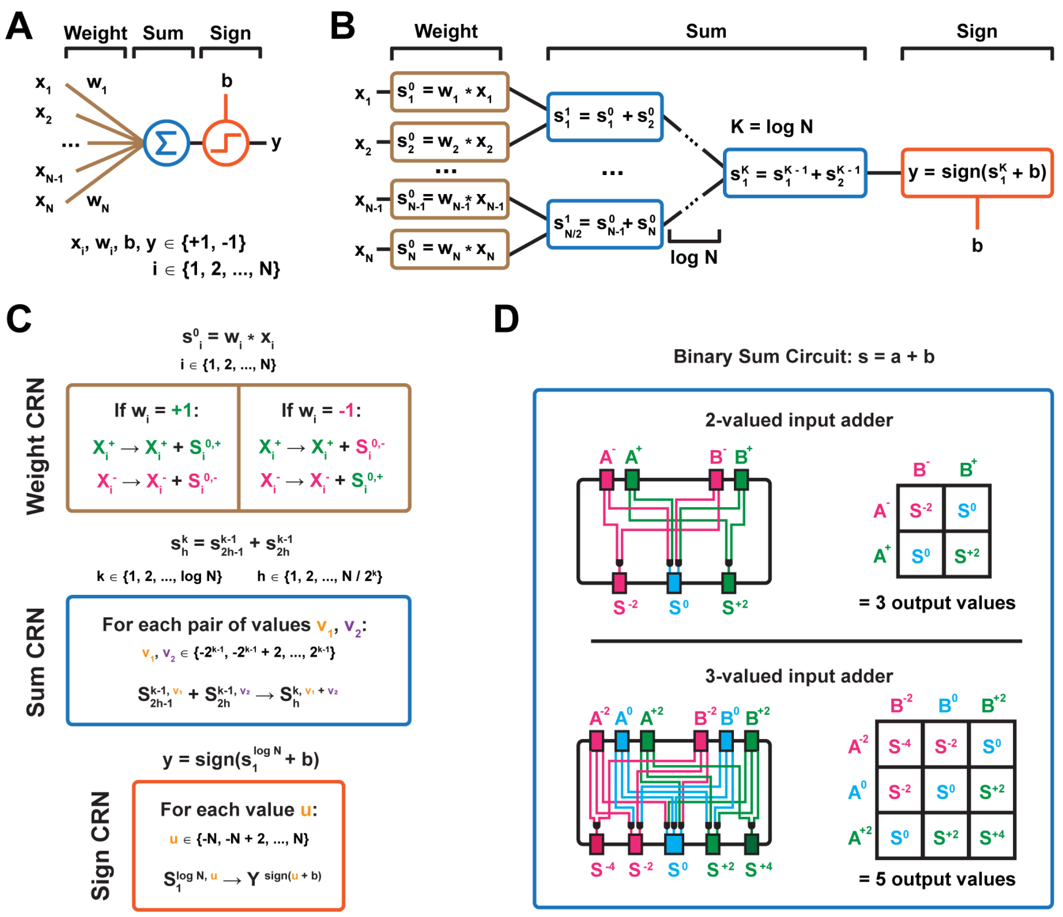

	B^-	B^+
A^-	S^{-2}	S^0
A^+	S^0	S^{+2}

	B^{-2}	B^0	B^{+2}
A^{-2}	S^{-4}	S^{-2}	S^0
A^0	S^{-2}	S^0	S^{+2}
A^{+2}	S^0	S^{+2}	S^{+4}

Figure 2 A Illustration of a binarized neuron. **B** Computational graph of a binarized neuron. The binary summation tree (blue) has a depth of $\log(N)$. **C** Chemical reactions which implement the modules of the computational graph. **D** Example illustration of the binary addition circuit. A set of AND rules encode which input states (summands) correspond to what output state (sum).

values, $s^{k-1}_{2h-1}, s^{k-1}_{2h} \in \{v_1, ..., v_m\}$. We represent these states with species $S^{k-1,v_1}_{2h-1}, ..., S^{k-1,v_m}_{2h-1}$ and $S^{k-1,v_1}_{2h}, ..., S^{k-1,v_m}_{2h}$. For every combination of values v_i, v_j, add the following reaction (Figure 2C):

$$S^{k-1,v_i}_{2h-1} + S^{k-1,v_j}_{2h} \rightarrow S^{k,v_i+v_j}_{h}$$

Example logical circuits are illustrated in Figure 2D for $m = 2$ and $m = 3$. In general, if the input variables have cardinality m, we require m^2 reactions and the cardinality of the output variable becomes $2m - 1$. Note that this circuit is more similar to a demultiplexer than a carry adder.

Since each binary addition has depth 1, and there are $\log(N)$ levels of additions, the total depth is $\log(N)$. To calculate the total number of reactions, we first note that, at level k, there are $N/2^k$ additions. Each summand has cardinality $m = 2^{k-1} + 1$ (assuming binary-valued initial inputs). Hence, the total number of reactions across all $\log(N)$ levels can be calculated as a geometric series:

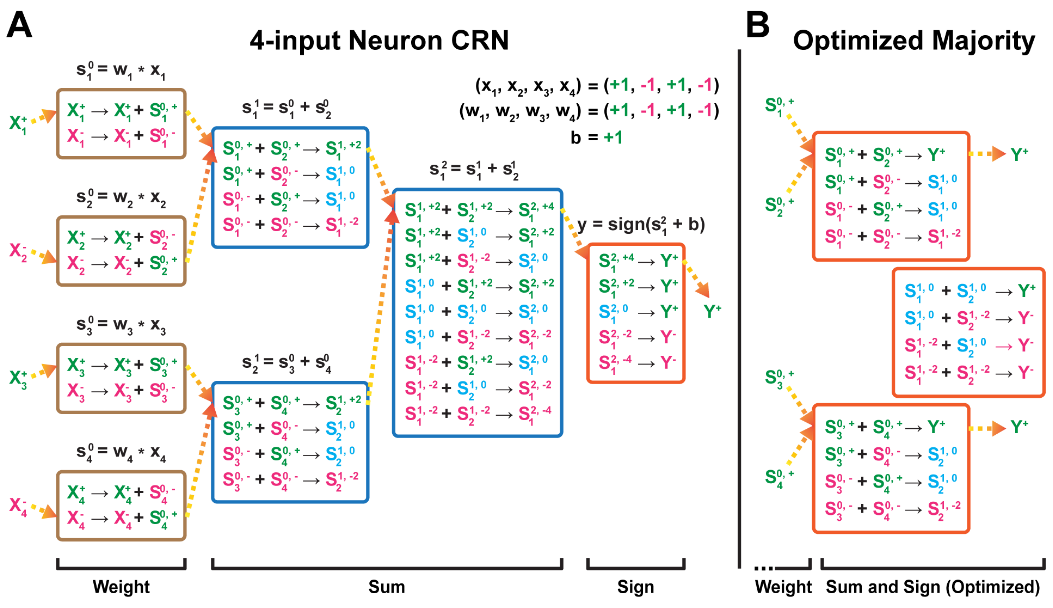

Figure 3 **A** Example CRN execution of a 4-input neuron. $(x_1, x_2, x_3, x_4) = (+1, -1, +1, -1)$ and $(w_1, w_2, w_3, w_4) = (+1, -1, +1, -1)$. **B** Optimized 4-input neuron (weight reactions are omitted).

$$\begin{aligned}\sum_{k=1}^{\log(N)} N \cdot \frac{(2^{k-1}+1)^2}{2^k} &= N \cdot \sum_{k=0}^{\log(N)-1} \frac{2^{2k}+2^{k+1}+1}{2^k} \\ &= \frac{N^2}{2} + N \cdot \log(N) + \frac{N}{2} - 1 \\ &= \mathcal{O}(N^2)\end{aligned}$$

We have thus shown that we can construct a digital sum circuit as a balanced binary tree of chemical reactions with $\mathcal{O}(\log(N))$ depth and $\mathcal{O}(N^2)$ reactions. We finalize the majority voting circuit by adding uni-molecular reactions translating every possible state species $S_1^{\log(N),-N}, \ldots, S_1^{\log(N),+N}$ of the final sum $s_1^{\log(N)}$ into the correct signed output species Y^+ or Y^- (N reactions):

$$S_1^{\log(N),v} \to Y^{\mathrm{sign}(v+b)}$$

4.3 An Illustrative Example: A 4-Input Binarized Neuron

We show the digital CRN of a 4-input binarized neuron in Figure 3A, which carries out the full sum before applying the sign reaction. However, we are ultimately not interested in computing the sum of input species, only their majority vote. If the absolute value of the partial sum in any of the sub trees is greater than $N/2$, we can stop computing the sum since the majority is already determined. That is, if $|v_i + v_j + b| > N/2$, alter the reaction to immediately produce the output species Y^+ or Y^-:

$$S_{2h-1}^{k-1,v_i} + S_{2h}^{k-1,v_j} \to Y^{\mathrm{sign}(v_i+v_j+b)}$$

Table 1 Number of CRN reactions required to compute N-input digital majority.

N	2	4	8	16	32
# Reactions	4	12	50	182	654

Similarly, it is unnecessary to translate the final sums into their corresponding signs with separate uni-molecular reactions; we can immediately produce the output species Y^+, Y^- from the last level of sums. An optimized 4-input binarized neuron is illustrated in Figure 3B. The optimization reduces the input cardinality of the two summands at the final level by 1. Using the geometric series defined in Section 4.2, we can calculate the number of removed reactions at level $k = \log(N)$:

$$N \cdot \frac{(2^{\log(N)-1}+1)^2}{2^{\log(N)}} - N \cdot \frac{(2^{\log(N)-1})^2}{2^{\log(N)}} = N + 1$$

The optimized circuit thus requires $\frac{N^2}{2} + N \cdot \log(N) - \frac{N}{2} - 2$ reactions to compute digital majority. Table 1 lists the number of required reactions up to $N = 32$ inputs.

4.4 DNA Strand Displacement Design

Here we present the DNA strand displacement (DSD) implementation of the digital BNN CRN. The implementation is based on the *two-domain* design of [3]. The complete DSD schematic is shown in Figure 4. The implementation is described in detail below.

Each activation x_i^l in layer l is represented by two input strands, $X_i^{l,+}$ and $X_i^{l,-}$. For each weighted connection $s_{i,j}^{l,0} = w_{i,j}^l \cdot x_i^{l-1}$, we add four gates. If $w_{i,j}^l = +1$, we add the following gates:

1. Gate $G_{\text{Weight},i,j}^{l,+}$, which outputs $K_i^{l-1,+}$ and $S_{i,j}^{l,0,+}$ given the strand $X_i^{l-1,+}$ as input.
2. Gate $G_{\text{Restore},i}^{l-1,+}$, which translates $K_i^{l-1,+}$ back to $X_i^{l-1,+}$.
3. Gate $G_{\text{Weight},i,j}^{l,-}$, which outputs $K_i^{l-1,+}$ and $S_{i,j}^{l,0,-}$ given the strand $X_i^{l-1,+}$ as input.
4. Gate $G_{\text{Restore},i}^{l-1,-}$, which translates $K_i^{l-1,-}$ back to $X_i^{l-1,-}$.

If $w_{i,j}^l = -1$, we swap the output strands $S_{i,j}^{l,0,+}$ and $S_{i,j}^{l,0,-}$ such that they are released by gates $G_{\text{Weight},i,j}^{l,-}$ and $G_{\text{Weight},i,j}^{l,+}$ respectively. Next, we add a cascade of AND gates to implement $s_j^l = \sum_{i=1}^{N^{l-1}} s_i^{l,0}$. For each binary addition $s_{h,j}^{l,k} = s_{2h-1,j}^{l,k-1} + s_{2h,j}^{l,k-1}$, for all M^2 combinations of summand values v_{m_1}, v_{m_2}, we add:

1. Gate $G_{\text{Sum},h,j}^{l,k,m_1,m_2}$, which outputs $S_{h,j}^{l,k,v_{m_1}+v_{m_2}}$ given $S_{2h-1,j}^{l,k-1,v_{m_1}}$ and $S_{2h,j}^{l,k-1,v_{m_2}}$ as input.

However, if $k = \log(N^{l-1})$ (the final tree level), or if $|s_{2h-1,j}^{l,k-1} + s_{2h,j}^{l,k-1} + b_j^l| > N^{l-1}/2$, we let $G_{\text{Sum},h,j}^{l,k,m_1,m_2}$ produce the neuron majority species $X_j^{l,+}$ or $X_j^{l,-}$.

Note that, since the output strand of each two-domain gate reverses orientation as compared to its input strand(s) (the toehold moves to the opposite side of the recognition domain), we have to alternate the orientation of gates at each level in the summation tree. Also, since the summation can end at either an odd or- even numbered level, we have to add translator gates which swap the orientation of the final activation species $X_j^{l,+}$ and $X_j^{l,-}$. This guarantees that the activation output strands are always in the correct orientation with respect to the input weight gates of the next layer.

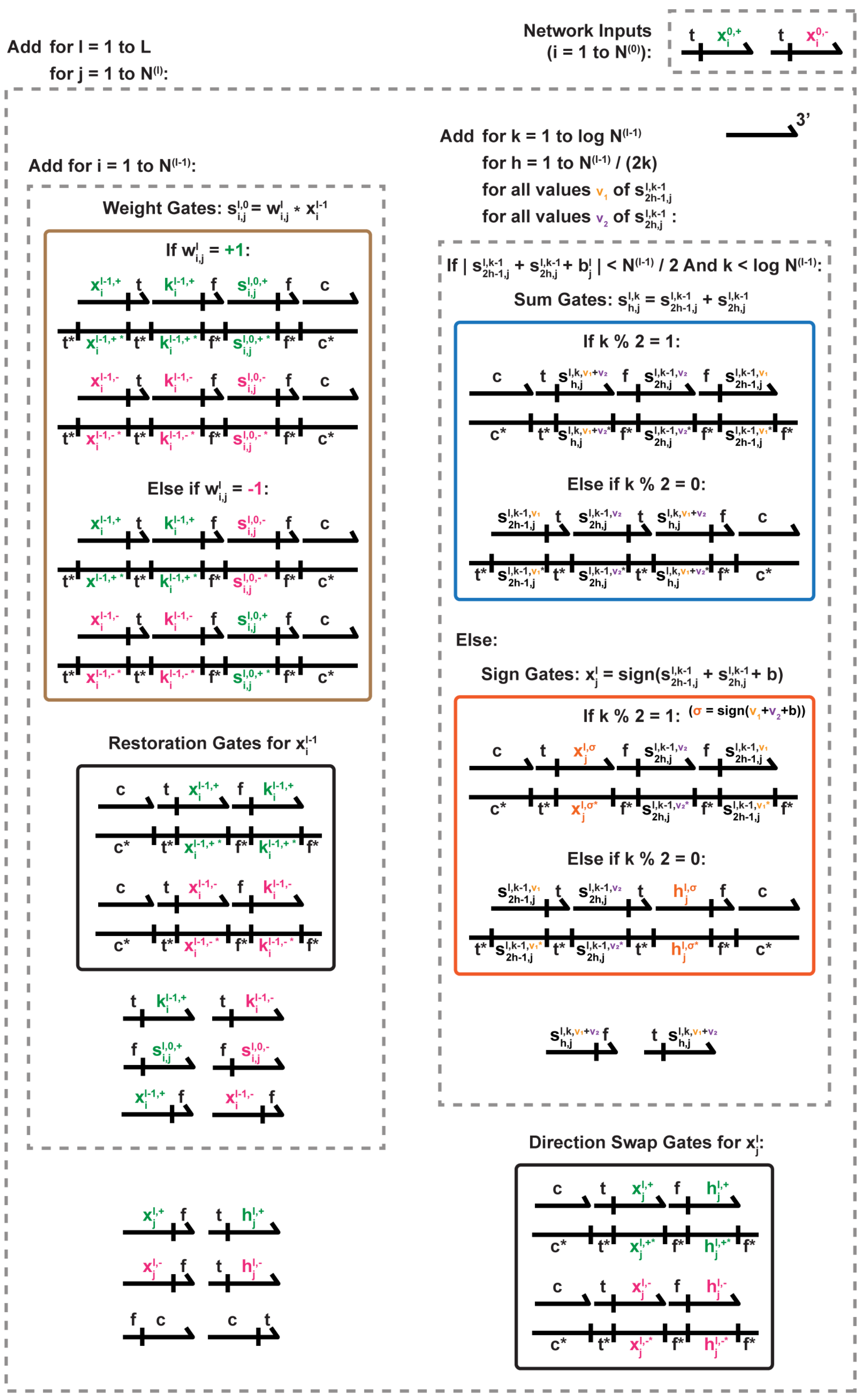

Figure 4 DSD schematic of the binarized neural network implementation, based on the two-domain architecture of [3].

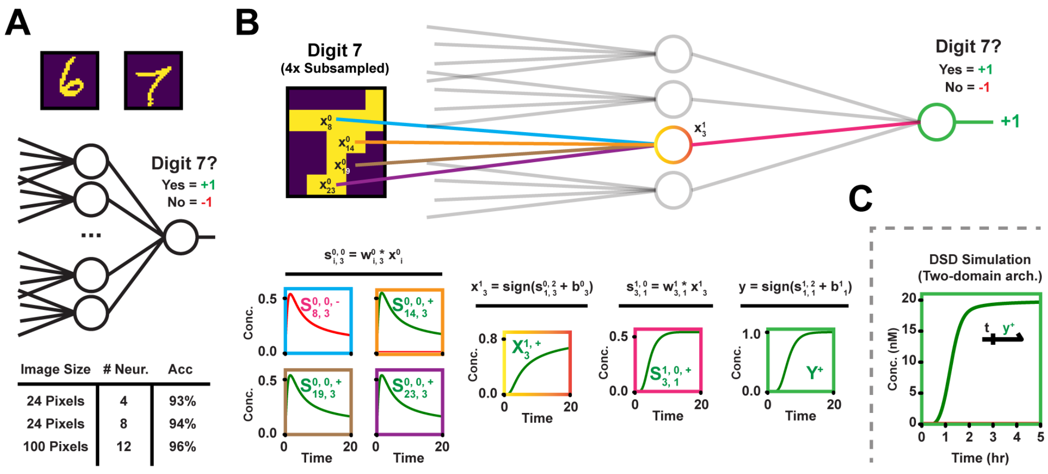

Image Size	# Neur.	Acc
24 Pixels	4	93%
24 Pixels	8	94%
100 Pixels	12	96%

Figure 5 A A single-hidden layer network with 4, 8 or 12 neurons was trained to classify MNIST digits 6 vs. 7. **B** Example CRN simulation, as a system of ODEs with unit concentrations and reaction rates. Graph color corresponds to network component. **C** The network was simulated in Microsoft's DSD tool. Signal concentration = 20nM. Shown is the final output strand trajectory.

5 Experiments

5.1 MNIST Simulations

We demonstrate our binarized neural network design on the MNIST digit classification task. Similar to one of the analyses in [8], we tested the model's ability to distinguish between digits 6 and 7. We trained three versions of a single-hidden layer network (Figure 5A), with 4, 8 and 12 hidden neurons respectively. For the 4 and- 8 hidden neuron networks, we downsampled the input images to 5×5 pixels. For the 12 neuron version, the images were downsampled to 10×10 pixels. The image pixel values were binarized by subtracting the mean pixel intensity and thresholding at 0. We settled on a sparse connectivity structure, where neurons were connected to 4 randomly chosen inputs. The networks were trained following the procedure of [14], using PyTorch [21] and the Adam optimizer [15].

The network with only 4 hidden neurons correctly classified as many as 93% of test images (Figure 5A, bottom table). Test accuracy increased marginally up to 96% for the largest network. We translated the 4-hidden neuron network into our digital CRN design, totalling 192 molecular species and 102 reactions, and simulated the entire system of ODEs for an example input image (Figure 5B). Finally, we mapped the 4-hidden neuron network CRN to a DNA strand displacement (DSD) cascade, using the architecture presented in Section 4.4. The DSD specification was compiled into a system of ODEs using Microsoft's DSD tool with default toehold binding rates and "infinite" compilation mode [17]. The ODE was simulated by Python SciPy's *odeint* (Figure 5B).

5.2 Noise Tolerance Simulations

Next, we compared our digital design (d-BNN) to an analog rate-independent design (a-BNN) with the HardTanh activation function defined in Section 2.2. The designs were compiled into CRNs using Microsoft's DSD tool. Each CRN was copied to Python, compiled into ODEs and simulated by SciPy's odeint. Keeping the designs as CRNs in Python allows us to easily add leak pathways. We provide the schematic for the analog HardTanh network as idealized CRNs in Appendix B and as DNA strand displacement cascades in Appendix C.

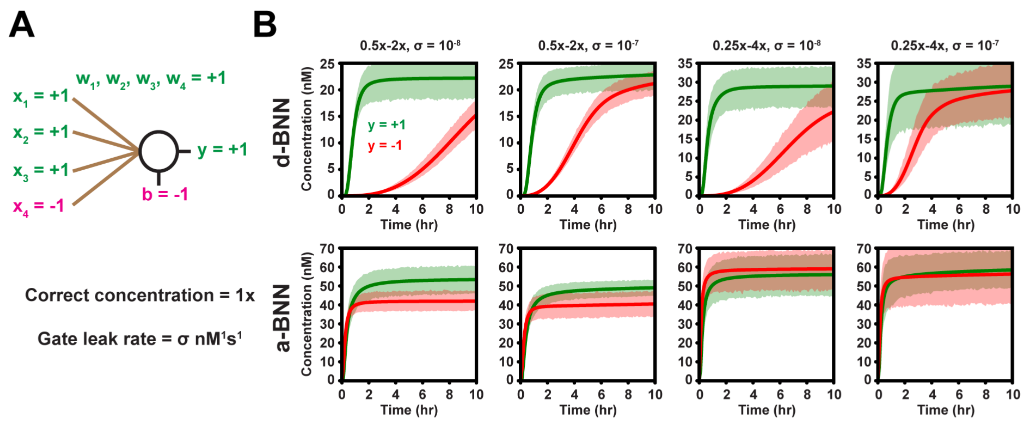

Figure 6 **A** A single 4-input neuron was compiled into DSD (both as a digital circuit – d-BNN, and as an analog circuit – a-BNN). Shown is the tested input pattern. **B** Noise- and leak tolerance simulations. Concentrations varied uniformly between 0.5x-2x or 0.25x-4x. Signal concentration (1x) = 20nM. Leak reactions were added to DSD gates with rates of 10^{-8} or 10^{-7} $\text{nM}^{-1}\text{s}^{-1}$. Each simulation was run 10 times. 95% confidence intervals estimated from 1000-fold bootstrapping.

We compared the effects of concentration noise and gate leak on each respective design for a single 4-input neuron (Figure 6A). Specifically, we multiplied input strand and gate concentrations with a uniform random value and added leak reactions to all gates. Four different conditions were tested, and each condition was simulated 10 times. The results indicate that the digital binarized neuron is more robust than its analog counterpart (Figure 6B); in all four conditions, the correct "turned-on" output trajectory is separable from the "turned-off" (leaked) trajectory up to 3 hours for the digital neuron, whereas the analog neuron looses separability of the output trajectories almost immediately.

5.3 Physical Experimental Results

We performed wet lab experiments to validate the function of the basic DSD components used in the BNN. In Figure 7A, we tested a single catalytic two-domain weight gate, which is used to restore the input signal to the operating concentration (4nM) given different concentrations of input strand. As can be seen, the gate restores the signal with low levels of leak, and all conditions reach 75% of the target concentration within 12 hours. In Figure 7B, we tested the function of a simple 2-input majority voter where the bias term b is set to +1. The experiment suggests that the system functions correctly with low levels of leak. Note that there is no catalytic amplification of the majority voting output signal in Figure 7B, which is why the concentration is not restored to 4nM.

6 Discussion

When comparing digital BNNs to other molecular neural network implementations, our design offers both advantages and disadvantages. In terms of complexity, our design is less efficient (compact) than both rate-dependent and rate-independent analog designs [23, 8, 32], which require $\mathcal{O}(N)$ bi-molecular reactions for weighting and only $\mathcal{O}(1)$ reactions for majority voting. However, our simulations indicate that the digital design is more robust to concentration noise and gate leak compared to analog implementations. Furthermore, since rate-independent analog CRNs operate on monotonic dual-rail species, any physical implementation of a

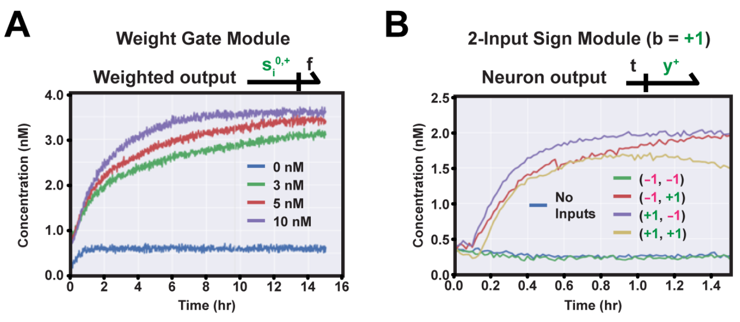

Figure 7 **A** An amplifier is used to restore the operating concentration (4nM) of the input strand given different input strand concentrations. **B** A 2-input majority voting circuit with +1 bias is used to trigger the output strand only if the positive inputs are in majority. Input concentration is 4nM.

deep, fully connected neural network would require an exponentially large concentration of molecular substrates at the final network layers (exponential in the network layers). The digital design, however, allows a constant substrate concentration across all layers.

The DSD architecture of the digital BNN can potentially support even large networks, since the DNA gates can be enzymatically prepared from a pool of fully double-stranded DNA [7]. However, it is often difficult in practice to scale up the number of two-domain gates in a single reaction vessel due to the many possible leak pathways, in particular for catalytic gates. To reduce noise, we might consider isolating each neuron computation with either localized reactions [2] or physical separation by microfluidic droplets [31]. Alternatively, strand-displacing polymerase (PSD) may be a promising option, which leak minimally [29, 25]. Furthermore, all reactions can be implemented with single-stranded PSD AND-gates, allowing for simple large-scale synthesis. The main caveat is that PSD currently does not support catalytic reactions. However, we can forego the catalytic reactions and instead start with exponentially large input concentrations, which may be feasible for 1–2 hidden layers of computation.

Finally, for future work we wonder whether the gate complexity of $\mathcal{O}(N^2)$ for digital majority voting can be reduced by acknowledging that neural networks often behave well with small errors. We thus ask if we could design an "approximate" majority voter with $\mathcal{O}(N)$ gates. For example, instead of computing exact partial sums on groups of inputs, we might get approximately correct output using only the signs of the inputs at each level of the tree.

7 Conclusion

In this paper, we present a digital molecular design of binarized neural networks. We devise a depth-optimal majority voting circuit that uses $\mathcal{O}(N^2)$ bi-molecular chemical reactions in a cascade of depth $\mathcal{O}(\log(N))$ to compute N-input majority. Each neuron uses this circuit to compute its activation function. We demonstrated our molecular implementation on the MNIST digit classification task, by simulating the ODE of a network with 4 hidden neurons as a DNA strand displacement cascade. We further demonstrated improved tolerance to concentration noise compared to analog BNN implementations in simulations.

We hope this paper sparks future research in molecular implementations of machine learning models. The intersection of digital circuit design, ML techniques and chemical reaction networks can enable other computational models implemented as molecular circuits and lead to whole new applications in molecular computing.

References

1 Y. Benenson, B. Gil, U. Ben-Dor, R. Adar, and E. Shapiro. An autonomous molecular computer for logical control of gene expression. *Nature*, 429(6990):423–429, 2004.

2 H. Bui, S. Shah, R. Mokhtar, T. Song, S. Garg, and J. Reif. Localized DNA hybridization chain reactions on DNA origami. *ACS nano*, 12(2):1146–1155, 2018.

3 L. Cardelli. Two-domain DNA strand displacement. *Mathematical Structures in Computer Science*, 23(2):247–271, 2013.

4 L. Ceze, J. Nivala, and K. Strauss. Molecular digital data storage using dna. *Nature Reviews Genetics*, 20(8):456–466, 2019.

5 H.L. Chen, D. Doty, and D. Soloveichik. Rate-independent computation in continuous chemical reaction networks. *In Proceedings of the 5th Conference on Innovations in Theoretical Computer Science*, pages 313–326, 2014 January.

6 S.X. Chen and G. Seelig. A DNA neural network constructed from molecular variable gain amplifiers. *In International Conference on DNA-Based Computers*, pages 110–121, 2017 September.

7 Y.J. Chen, N. Dalchau, N. Srinivas, A. Phillips, L. Cardelli, D. Soloveichik, and G. Seelig. Programmable chemical controllers made from DNA. *Nature nanotechnology*, 8(10):755–762, 2013.

8 K.M. Cherry and L. Qian. Scaling up molecular pattern recognition with DNA-based winner-take-all neural networks. *Nature*, 559(7714):370–376, 2018.

9 G.M. Church, Y. Gao, and S. Kosuri. Next-generation digital information storage in DNA. *Science*, 337(6102):1628–1628, 2012.

10 S. Darabi, M. Belbahri, M. Courbariaux, and V.P. Nia. BNN+: Improved binary network training. *OpenReview*, 2018.

11 I.R. Epstein and J.A. Pojman. An introduction to nonlinear chemical dynamics: Oscillations, waves, patterns, and chaos. *Oxford Univ Press London*, page London, 1998.

12 F. Fages, G. Le Guludec, O. Bournez, and A. Pouly. Strong turing completeness of continuous chemical reaction networks and compilation of mixed analog-digital programs. *In International Conference on Computational Methods in Systems Biology*, pages 108–127, 2017 September.

13 A. Hjelmfelt, E.D. Weinberger, and J. Ross. Chemical implementation of neural networks and turing machines. *Proceedings of the National Academy of Sciences*, 88(24):10983–10987, 1991.

14 I. Hubara, M. Courbariaux, D. Soudry, R. El-Yaniv, and Y. Bengio. Binarized neural networks. *In Advances in Neural Information Processing Systems*, pages 4107–4115, 2016.

15 D.P. Kingma and J. Ba. Adam: A method for stochastic optimization. *arXiv*, 2014. `arXiv:1412.6980`.

16 M.R. Lakin and A. Phillips. Modelling, simulating and verifying turing-powerful strand displacement systems. *In International Workshop on DNA-Based Computers*, pages 130–144, 2011 September.

17 M.R. Lakin, S. Youssef, F. Polo, S. Emmott, and A. Phillips. Visual DSD: a design and analysis tool for DNA strand displacement systems. *Bioinformatics*, 27(22):3211–3213, 2011.

18 R. Lopez, R. Wang, and G. Seelig. A molecular multi-gene classifier for disease diagnostics. *Nature chemistry*, 10(7):746–754, 2018.

19 M.O. Magnasco. Chemical kinetics is turing universal. *Physical Review Letters*, 78(6):1190, 1997.

20 L. Organick, S.D. Ang, Y.J. Chen, R. Lopez, S. Yekhanin, K. Makarychev, M.Z. Racz, G. Kamath, P. Gopalan, B. Nguyen, and C.N.etal. Takahashi. Random access in large-scale DNA data storage. *Nature biotechnology*, 36(3):242, 2018.

21 A. Paszke, S. Gross, S. Chintala, G. Chanan, E. Yang, Z. DeVito, Z. Lin, A. Desmaison, L. Antiga, and A. Lerer. Automatic differentiation in pytorch, 2017.

22 L. Qian and E. Winfree. Scaling up digital circuit computation with DNA strand displacement cascades. *Science*, 332(6034):1196–1201, 2011.

23 L. Qian, E. Winfree, and J. Bruck. Neural network computation with DNA strand displacement cascades. *Nature*, 475(7356):368–372, 2011.

24 P. Senum and M. Riedel. Rate-independent constructs for chemical computation. *PloS one*, 6(6):e21414, 2011.

25 S. Shah, J. Wee, T. Song, L. Ceze, K. Strauss, Y.J. Chen, and J. Reif. Using strand displacing polymerase to program chemical reaction networks. *Journal of the American Chemical Society*, 142(21):9587–9593, 2020.

26 T. Simons and D.J. Lee. A review of binarized neural networks. *Electronics*, 8(6):661, 2019.

27 D. Soloveichik, M. Cook, E. Winfree, and J. Bruck. Computation with finite stochastic chemical reaction networks. *Natural Computing*, 7(4):615–633, 2008.

28 D. Soloveichik, G. Seelig, and E. Winfree. DNA as a universal substrate for chemical kinetics. *Proceedings of the National Academy of Sciences*, 107(12):5393–5398, 2010.

29 T. Song, A. Eshra, S. Shah, H. Bui, D. Fu, M. Yang, R. Mokhtar, and J. Reif. Fast and compact DNA logic circuits based on single-stranded gates using strand-displacing polymerase. *Nature nanotechnology*, 14(11):1075–1081, 2019.

30 N. Srinivas, J. Parkin, G. Seelig, E. Winfree, and D. Soloveichik. Enzyme-free nucleic acid dynamical systems. *Science*, 358(6369), 2017.

31 A. Stephenson, M. Willsey, J. McBride, S. Newman, B. Nguyen, C. Takahashi, K. Strauss, and L. Ceze. PurpleDrop: A digital microfluidics-based platform for hybrid molecular-electronics applications. *IEEE Micro*, 40(5):76–86, 2020.

32 M. Vasic, C. Chalk, S. Khurshid, and D. Soloveichik. Deep molecular programming: A natural implementation of binary-weight ReLU neural networks. *arXiv*, 2020. `arXiv:2003.13720`.

33 M. Vasic, D. Soloveichik, and S. Khurshid. CRN++: Molecular programming language. *In International Conference on DNA Computing and Molecular Programming*, pages 1–18, 2018 October.

34 D.Y. Zhang and G. Seelig. DNA-based fixed gain amplifiers and linear classifier circuits. *In International Workshop on DNA-Based Computers*, pages 176–186, 2010 June.

A Generalized CRN Definition for Multi-layered Digital BNN

In this appendix, we extend the CRN formalism defined in Section 4 from a single binarized neuron to an arbitrarily sized network consisting of multiple neurons across many layers. Let us first extend the notation of the in-silico computational model, which, to remind the reader, is based on deterministic binarized neural networks (BNNs) as described by [14] with the added constraint that the number of neurons in any layer is a power of 2.

Let L be the number of network layers and let N^l be the number of neurons in layer l. Define $x_i^{(l)} \in \{+1, -1\}$ as the binary-valued activation of neuron i in layer l or, if $l = 0$, let $x_i^{(0)}$ be the i:th input to the network. Neuron i in layer $l - 1$ is connected to neuron j of layer l through the binary-valued weight $w_{i,j}^{(l)} \in \{+1, -1\}$. Additionally, Neuron j of layer l has an associated bias term (intercept) $b_j^{(l)} \in \{+1, -1\}$. We define activation $x_j^{(l)}$ of neuron j recursively as:

$$x_j^{(l)} = \begin{cases} +1 & \text{if } b_j^{(l)} + \sum_{i=1}^{N^{l-1}} w_{i,j}^{(l)} \cdot x_i^{(l-1)} > 0 \\ -1 & \text{else} \end{cases}$$

CRN Definition

Each neuron activation x_i^l is represented by two CRN species $X_i^{l,+}$ and $X_i^{l,-}$, corresponding to states $x_i^l = +1$ and $x_i^l = -1$ respectively. For each weight operation $s_{i,j}^{l,0} = w_{i,j}^l \cdot x_i^{l-1}$, add either of the following sets of reactions based on the sign of $w_{i,j}^l$:

If $w^l_{i,j} = +1$:

$$X_i^{l-1,+} \to X_i^{l-1,+} + S_{i,j}^{l,0,+}$$
$$X_i^{l-1,-} \to X_i^{l-1,-} + S_{i,j}^{l,0,-}$$

Else if $w^l_{i,j} = -1$:

$$X_i^{l-1,+} \to X_i^{l-1,+} + S_{i,j}^{l,0,-}$$
$$X_i^{l-1,-} \to X_i^{l-1,-} + S_{i,j}^{l,0,+}$$

The sum operation $s^l_j = \sum_{i=1}^{N^{l-1}} s_i^{l,0}$ is calculated as a balanced tree of binary additions using the following recursive definition:

$$s_{h,j}^{l,k} = s_{2h-1,j}^{l,k-1} + s_{2h,j}^{l,k-1}$$

Here $k = 1, ..., \log(N^{l-1})$ denotes the current depth in the tree and $h = 1, ..., N^{l-1}/2^k$ denotes the tree node. Assume each summand can take on M discrete values, $s_{2h-1,j}^{l,k-1}, s_{2h,j}^{l,k-1} \in \{v_1, ..., v_M\}$. The resulting sum can take on $2M-1$ values, $s_{h,j}^{l,k} \in \{v_1+v_1, v_1+v_2, ..., v_M+v_M\}$. We represent each discrete state of each variable with a distinct molecular species:

State $s_{h,j}^{l,k} = v_m$ is encoded by species $S_{h,j}^{l,k,v_m}$

For each of the M^2 combinations of summand values $s_{2h-1,j}^{l,k-1} = v_{m_1}$, $s_{2h,j}^{l,k-1} = v_{m_2}$, add the reaction:

$$S_{2h-1,j}^{l,k-1,v_{m_1}} + S_{2h,j}^{l,k-1,v_{m_2}} \to S_{h,j}^{l,k,v_{m_1}+v_{m_2}}$$

At depth $\log(N^{l-1})$ in the tree, the final weighted sum will be stored in variable $s_{1,j}^{l,\log(N^{l-1})}$. To compute the binary threshold activation function of neuron j in layer l, which we represent with species $X_j^{l,+}$ and $X_j^{l,-}$, add the following reaction for each of the $N+1$ possible sum output species $S_{1,j}^{l,\log(N),-N}, ..., S_{1,j}^{l,\log(N),+N}$ (recalling that b^l_j is the bias term for neuron j in layer l):

$$S_{1,j}^{l,\log(N),v} \to X_j^{l,\mathrm{sign}(v+b^l_j)}$$

B Analog Rate-Independent HardTanh Network CRN

In the main paper, we compare the digital CRN of a binary-threshold neuron to an analog CRN implementation of a HardTanh-activated neuron. Here, we describe the analog design, including idealized CRN reactions and the two-domain DSD schematic. The implementation is based on the rate-independent neural network CRN that was recently proposed by [32], but with a HardTanh activation function $\min(\max(x, -1), 1)$ instead of the ReLU function $\max(x, 0)$.

In analog CRN computing, the weight and- sum operations are performed simultaneously. We implement the weighted sum of neuron j,

$$s^l_j = \sum_{i=1}^{N^{l-1}} w^l_{i,j} \cdot x^l_i$$

by adding either of the following two sets of reactions for each input i:

If $w^l_{i,j} = +1$:

$$X^{l-1,\log(N^l),+}_{i,j} \rightarrow S^{l,+}_j$$
$$X^{l-1,\log(N^l),-}_{i,j} \rightarrow S^{l,-}_j$$

Else if $w^l_{i,j} = -1$:

$$X^{l-1,\log(N^l),+}_{i,j} \rightarrow S^{l,-}_j$$
$$X^{l-1,\log(N^l),-}_{i,j} \rightarrow S^{l,+}_j$$

Note that the molecular species for input x^{l-1}_i are indexed by j. We cannot use catalytic reactions for rate-independent monotonic CRNs, which means we have to make individual copies of x^{l-1}_i for each outgoing neuron j. Further down in this text, we will add fan-out reactions which create as many copies of x^l_j as needed by the next layer. This copy operation, which is implemented as a binary tree, is the reason for having the hard-coded superscript $\log(N^l)$ in the species notation. Also note that the bias term b^l_j is implemented by setting the initial concentrations of $S^{l,+}_j$ and $S^{l,-}_j$ appropriately; if $b^l_j = +1$, start with $s^{l,+}_j(0) = 1$, or if $b^l_j = -1$, start with $s^{l,-}_j(0) = 1$.
Next, we implement the HardTanh activation function,

$$x^l_j = \min(\max(s^l_j, -1), 1)$$

by stacking the monotonic, dual-rail reaction set of the two functions $h^l_j = \max(s^l_j, -k)$ and $x^l_j = \min(h^l_j, m)$ as described by [5]:

$$\begin{aligned} S^{l,+}_j &\rightarrow H^{l,+}_j + K^l_j \\ S^{l,-}_j + K^l_j &\rightarrow H^{l,-}_j \\ H^{l,-}_j &\rightarrow X^{l,0,-}_{j,1} + M^l_j \\ H^{l,+}_j + M^l_j &\rightarrow X^{l,0,+}_{j,1} \end{aligned}$$

In order for these reactions to implement clipping of s^l_j at [-1, 1], we have to start with initial concentrations $k^l_j(0) = 1$ and $m^l_j(0) = 1$.

Finally, we fan out activation x^l_j to the outgoing N^{l+1} neurons of the next layer, by implementing copy operations $x^l_{j,k} = x^l_j$, $1 \leq k \leq N^{l+1}$. Since we only allow reactions with at most 2 products, we have to perform the copy in a balanced binary tree of depth of $\log(N^{l+1})$. Specifically, for $d = 1$ to $\log(N^{l+1})$ and $k = 1$ to 2^{d-1}, add the following two reactions:

$$X^{l,d-1,+}_{j,k} \rightarrow X^{l,d,+}_{j,2k} + X^{l,d,+}_{j,2k+1}$$
$$X^{l,d-1,-}_{j,k} \rightarrow X^{l,d,-}_{j,2k} + X^{l,d,-}_{j,2k+1}$$

To demonstrate the operation of the analog HardTanh CRN, we compiled the same 4-neuron network that was used in Figure 5 and simulated the resulting system of ODEs when classifying MNIST digit 7 from 6 (Figure 8A). Here, the monotonic dual-rail computation of the HardTanh function will make it so that the steady state concentration of the correct network output species (in this case $X^{2,0,+}_{1,1}$) is exactly 1 unit larger than the concentration of the minority species ($X^{2,0,-}_{1,1}$).

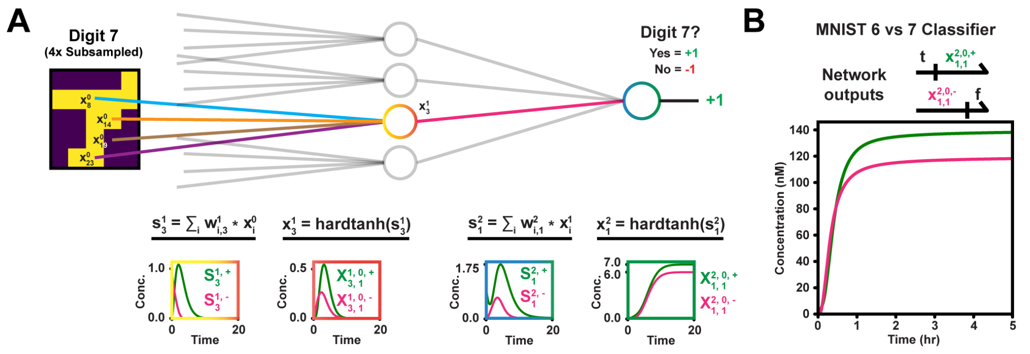

Figure 8 **A** Example CRN simulation, as a system of ODEs with unit concentrations and reaction rates. Graph color corresponds to network component. **B** The network was compiled into DSD gates and simulated in Microsoft's DSD tool. The graph shows the trajectory of the final output strand.

C Analog HardTanh BNN DSD Schematic

The DSD schematic for the analog HardTanh network is shown in Figure 9. Each activation x_i^l (before fanning out) is represented by two input strands, $X_{i,1}^{l,0,+}$ and $X_{i,1}^{l,0,-}$. Immediately following the network input strands $X_{i,1}^{0,0,+}$ and $X_{i,1}^{0,0,+}$, we add a cascade of gates which create N^1 copies of $X_{i,1}^{0,0,+}$ and $X_{i,1}^{0,0,-}$. For $d = 1$ to $\log(N^l)$ and $h = 1$ to 2^{d-1}, we add:

1. Gate $G_{\text{Fanout},i,h}^{l,d,+}$, which translates $X_{i,h}^{l,d-1,+}$ to $X_{i,2h}^{l,d,+}$ and $X_{i,2h+1}^{l,d,+}$.

The N^l copies are now stored in the signal strands $X_{i,j}^{0,\log(N^1),+}$ and $X_{i,j}^{0,\log(N^1),+}$, $1 \leq j \leq N^1$. Note that we require different orientations for the negative and- positive signal strands; this is needed to make the Fork and- Join gates of the HardTanh circuit compatible without extra translators. Next, for each input i in the weighted sum $s_j^l = \sum_{i=1}^{N^{l-1}} w_{i,j}^l \cdot x_i^l$, we add either of the following two sets of gates depending on the sign of $w_{i,j}^l$:
If $w_{i,j}^l = -1$, we add:

1. Gate $G_{\text{Weight},i,j}^{l,+}$ which outputs signal strand $S_j^{l,-}$.
2. Gate $G_{\text{Weight},i,j}^{l,-}$ which outputs signal strand $S_j^{l,+}$.

If $w_{i,j}^l = +1$, we must add an extra translation step in order to maintain the orientation of the output strands. We thus add:

1. Gate $G_{\text{Weight},i,j}^{l,+}$ which outputs signal strand $D_j^{l,+}$.
2. Gate $G_{\text{Weight},i,j}^{l,-}$ which outputs signal strand $D_j^{l,-}$.
3. Gate $G_{\text{Sum-Swap},j}^{l,+}$ which outputs $S_j^{l,+}$ given $D_j^{l,+}$ as input.
4. Gate $G_{\text{Sum-Swap},j}^{l,-}$ which outputs $S_j^{l,-}$ given $D_j^{l,-}$ as input.

The HardTanh circuit is implemented by adding a sequence of 4 gates:

1. Gate $G_{\text{HardTanh}_1,j}^{l}$, which outputs K_j^l and $H_j^{l,+}$ given $S_j^{l,+}$ as input.
2. Gate $G_{\text{HardTanh}_2,j}^{l}$, which outputs $H_j^{l,-}$ given $S_j^{l,-}$ and K_j^l as input.
3. Gate $G_{\text{HardTanh}_3,j}^{l}$, which outputs M_j^l and $X_{j,1}^{l,0,+}$ given $H_j^{l,-}$ as input.
4. Gate $G_{\text{HardTanh}_4,j}^{l}$, which outputs $X_{j,1}^{l,0,+}$ given $H_j^{l,+}$ and M_j^l and K_j^l as input.

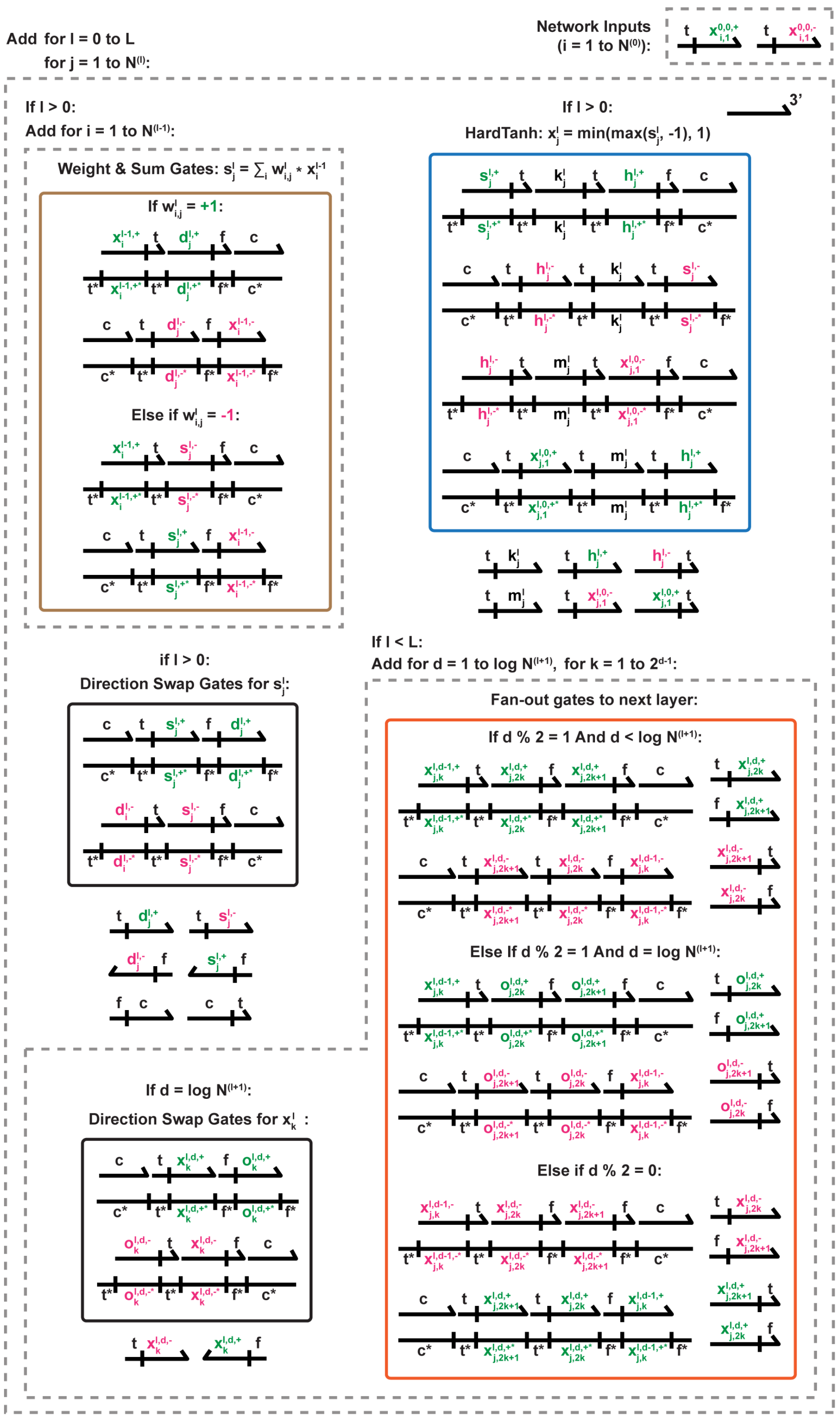
Add for l = 0 to L
for j = 1 to N(l):
Network Inputs (i = 1 to N(0)):
If l > 0:
Add for i = 1 to N(l-1):
Weight & Sum Gates: s_j^l = Σ_i w_{i,j}^l * x_i^{l-1}
If w_{i,j}^l = +1:
Else if w_{i,j}^l = -1:
If l > 0:
HardTanh: x_j^l = min(max(s_j^l, -1), 1)
3'
if l > 0:
Direction Swap Gates for s_j^l:
If l < L:
Add for d = 1 to log N(l+1), for k = 1 to 2^{d-1}:
Fan-out gates to next layer:
If d % 2 = 1 And d < log N(l+1):
Else If d % 2 = 1 And d = log N(l+1):
Else if d % 2 = 0:
If d = log N(l+1):
Direction Swap Gates for x_k^l :

Figure 9 DSD schematic of the analog HardTanh neural network implementation, based on the two-domain architecture of [3].

Finally, we add a cascade of fan-out gates which multiplex the neuron activation strands $X^{l,0,+}_{j,1}$ and $X^{l,0,-}_{j,1}$ to N^{l+1} copies, $X^{l,0,+}_{j,k}$ and $X^{l,0,+}_{j,k}$ (same set of gates $G^{l,d,+}_{\text{Fanout},j,k}$ and $G^{l,d,-}_{\text{Fanout},j,k}$ as previously described). We mind the orientation of positive and- negative signal strands by alternating gate orientation and add direction swap gates at the final layer in case the fan-out depth is odd-numbered.

We replicated the DSD simulation of the 4-neuron MNIST classifier of Figure 5C using the HardTanh circuit. The trajectories of the final output species $X^{2,0,+}_{1,1}$ and $X^{2,0,-}_{1,1}$ are shown in Figure 8B. We set the signal unit to 20 nM (same as the digital BNN in Figure 5C), which means that the final steady state concentrations become 140 nM and 120 nM (Compare to the unit-less steady-state concentrations of Figure 8A, which were 7 and 6 respectively).